Journal of Thermal Analysis and Calorimetry (2019) 136:1895–1904
https://doi.org/10.1007/s10973-018-7850-2

Stöber silica's microporosity

Insights from thermal analysis studies

Shanshan Li[1] · Quan Wan[2] · Zonghua Qin[2] · Yuhong Fu[2,3] · Yuantao Gu[2,3]

Received: 7 February 2018 / Accepted: 19 October 2018 / Published online: 1 November 2018

Abstract
Substantial knowledge gap still exists in understanding Stöber silica's confusing microporosity. In this work, we utilized simultaneous thermal analysis coupled with Fourier transform infrared spectroscopy to characterize Stöber silica samples prepared with various post-treatments including water or ethanol washing and drying at different temperatures. The results suggest that ammonia-catalyzed ethoxylation between ethanol and silanol groups can take place during drying, and the resulting ethoxyl groups along with Si-containing oligomers may contribute to serious micropore blocking. On the other hand, water washing is effective to hydrolyze and remove these pore-blocking materials and thus enable cleared micropores. Several interesting findings including the very sharp DSC peaks, high evolving temperature of ethanol, and pyrolysis of organic matters are linked to Stöber silica's micropores. Our work has undoubtedly improved the mechanistic understanding of Stöber silica's microporosity and will thus facilitate the practical optimization and application of this material.

Keywords Stöber silica · Post-treatment · Micropore · Pore blocking · Ethoxylation

Introduction

Stöber silica is a type of very important material featuring uniform spherical shape and monodispersed size distribution [1] and has been widely used in many studies and applications such as preparation of nanocomposites [2, 3], as photonic crystals [4], as a model material for investigation of silica's properties [5–7], etc. Since most of these applications stem from taking advantages of the external features, the size and monodispersity of Stöber silica particles have been extensively studied in previous researches [8–11]. However, it is now recognized that the internal porous structure of Stöber silica must be considered in many other applications including catalyst support [12], gene delivery [13] and even in some abovementioned applications.

Surprisingly, the descriptions of Stöber silica's internal structure were often confusing and contradictory. For example, the conventional nitrogen adsorption (− 196 °C) measurements revealed values of BET specific surface area (SSA) ranging from slightly larger than the geometric surface area indicating a nonporous structure [14–16] to much larger indicating a microporous structure [17, 18], which is summarized in Table 1 in our previous study [19]. Yet many other characterization methods (pycnometry, acid–base titration, liquid-phase adsorption, small-angle X-ray scattering, etc.) seem to favor a porous structure [14, 15, 20–22]. While the complexity of the internal structure was recorded in the literature as exemplified by a gel-like surface structure or a narrow sections of micropores [14] preventing access of N_2 molecules into internal pores and leading to the small BET SSA, an improved understanding of Stöber silica's internal structure is still much desired. It should be noticed that the

Electronic supplementary material The online version of this article (https://doi.org/10.1007/s10973-018-7850-2) contains supplementary material, which is available to authorized users.

✉ Quan Wan
wanquan@vip.gyig.ac.cn

[1] School of Chemistry and Materials Science, Guizhou Normal University, Guiyang 550001, Guizhou, China

[2] State Key Laboratory of Ore Deposit Geochemistry, Institute of Geochemistry, Chinese Academy of Sciences, Guiyang 550081, Guizhou, China

[3] University of Chinese Academy of Sciences, Beijing 100049, China

Table 1 The TG mass losses, C, N contents, BET SSAs and pore widths for all samples

Sample	TG mass loss/%		Element content/mass%		$S_{BET}/m^2\ g^{-1}$	Pore width/nm
	50–200 °C	200–1200 °C	C	N		
N-50	6.3	4.8	0.41	0.75	20.4	–
E-N	23.9	5.5	–	–	–	–
E-50	5.7	6.2	1.68	1.04	23.6	–
E-120	4.0	8.6	2.42	0.04	28.0	–
W-50	7.1	4.1	0.04	1.11	340.0	0.8
W-50 + 200	1.6	4.4	0.04	0.03	324.3	0.8
W-50 + 200 ~ E-50	7.0	5.5	1.77	0.01	322.6	1.3
W-50 + 200 ~ E(A)-50	6.3	6.5	2.27	0.20	Unfinished	–

misinterpretation of Stöber silica's microporosity may very likely by the reason for some misleading results, for example, an opposite trend in the size dependency of silica's SSA-normalized dissolution rate was mentioned due to the small BET SSA from N_2 adsorption [23].

We thus recently studied the Stöber silica's microporosity with an initial focus on the N_2 adsorption (− 196 °C) behavior and found that some often overlooked post-treatment processes significantly influenced the SSA of Stöber silica [19, 24]. Through careful control of the preparation conditions, we were able to obtain Stöber silica samples with BET SSA varying from several to about 350 $m^2\ g^{-1}$. Samples with large SSA (> 300 $m^2\ g^{-1}$) and short measurement time (< 3 days) normally required a deliberate combination of post-treatments, i.e., water (instead of ethanol) washing followed by gentle drying (e.g., initial 50 °C without vacuum). If the micropores were blocked to some extent, the measurement time would reach 1 month or even longer [24]. We proposed a pore blocking/clearing mechanism compatible with the aggregation plus monomer-addition silica growth model [9, 25, 26], which successfully explained all our experimental findings. Specifically, Stöber silica is prepared through hydrolysis and condensation of tetraethyl orthosilicate (TEOS) (see Eqs. S1, S2, and S3 in Supplementary Material). When the concentration of hydrolyzed TEOS monomer reaches a critical supersaturation level, the nucleation process takes place rapidly. Subsequently, the nuclei aggregate to generate larger particles, and the space among the nuclei form the micropores within the particles. In the meantime, the addition of TEOS monomer or oligomers to the particles surface occurs and may become the dominant process after nucleation terminates. As a consequence, the narrow micropore entrances or channels may be blocked with Si-containing monomer or oligomers at the later stage of particle growth. Besides, the condensation of hydroxyl groups, ethoxyl groups or dissolved Si species at the pore wall catalyzed by residual NH_3 also contributes to the pores blocking during drying [19]. Thus, whether a large BET SSA of a Stöber silica sample can be measured in a short time by N_2 adsorption highly depends on the effectiveness of pore clearing through suitable post-synthesis washing and drying processes.

Although the above mechanism works well to explain the effects of post-treatments on the N_2 adsorption results and is consistent with the elemental (C, N, and Si) analysis and TEM observation, we still focus on studying the relation of post-treatment and pores blocking or clearing and wish to find direct microscopic evidence and more manageable post-treatment processes with a view to improving the application of Stöber silica. Thus, we utilized the simultaneous thermal analysis (STA) coupled with Fourier transform infrared spectroscopy (FTIR) to systematically investigated the thermal behavior of Stöber silica samples prepared with different post-treatment conditions. The STA-FTIR technique is unique in its ability to conveniently determine the identity, amount and releasing temperature of volatile component from a sample (e.g., C- or N-containing species from Stöber silica particles), directly monitor the dynamic drying process and explicitly reveal certain special fluid properties under nanopore-confinement [27, 28]. The STA (TG/DSC) curves show the distinctive features such as the mass loss, the endothermic or exothermic process and temperature, etc. Interestingly, the results of STA-FTIR displayed the distinguishing features of samples varied with post-treatment (washing solvent, drying temperature and catalysis of NH_3). Therefore, we believe that our experimental results can provide substantial evidence to further enhance our understanding of Stöber silica's microporous structure. On the other hand, knowledge of Stöber silica's thermal properties will also prove very helpful in expanding its practical applications.

Experimental section

Materials

Tetraethyl orthosilicate (TEOS, 96%) was purchased from TCI (Shanghai) Development Co., Ltd., China. Ethanol (99.7%) was obtained from Sinopharm Chemical Reagent Company, China. Ammonia (~ 26.5%) was from Chongqing Chuanjiang Chemical Reagent Company, China. All these chemicals were used without further purification. Deionized water was obtained from a Millipore synergy UV system (resistivity, 18.2 MΩ cm).

Synthesis of Stöber silica

A mixture containing 191 mL of ethanol, 8.5 mL of ammonia and 26 mL of deionized water was stirred in a flask for approximately 45 min (20 °C). Subsequently, 14 mL of TEOS was quickly added to the mixture, which was continuously stirred for 80 min [8, 19]. The molar concentration of TEOS, NH_3 and H_2O was approximately 0.25, 0.5 and 7.5 M, respectively, assuming that all mixed liquid volumes were additive. After reaction, the mixture was centrifuged at 10,000 rpm (9940 g) to collect the white silica precipitate. According to transmission electron microscopic observations (see Fig. S1 in Supplementary Material for the representative sample W-50), the silica particles display the regular spherical shape and good size monodispersity. The diameter of particles is about 170 nm, and the geometric surface area is calculated to be 18.5 $m^2\ g^{-1}$ using the bulk density of 1.9 g cm^{-3} [21].

Post-treatment of samples

The above as-synthesized Stöber silica product was divided into 3 portions subject to different washing and drying processes. All the washing was performed 4 times using a vortex mixer, and the washing solvent (10 mL each time for collected product from 40 mL of suspension) was separated by centrifugation. Drying was performed for 2 h but at different temperatures. Figure 1 shows the detailed sample coding and corresponding process scheme for all 8 representative samples. Specifically, the first portion was directly dried at 50 °C without washing to get a sample denoted as N-50. The second portion was first washed with water and dried at 50 °C to make sample W-50, which was further dried at 200 °C to obtain sample W-50 + 200. After that, sample W-50 + 200 was washed with ethanol (with or without ammonia) and dried at 50 °C to obtain samples W-50 + 200 ~ E-50 and W-50 + 200 ~ E(A)-50, respectively. The third portion was washed with ethanol and then went through no drying, 50 °C drying, and 120 °C drying. The resulting samples were denoted as E-N, E-50 and E-120, respectively.

Generally, the drying temperature during synthesis of Stöber silica was lower than 200 °C [8, 14, 15].Thus we chose the 50 °C (low), 120 °C (moderate) and 200 °C (high) as the main drying temperature. Water washing could hydrolyze the surface ethoxyl group, and the DSC curves had no obvious difference under the above temperature. Therefore after water washing, the 50 °C was adopted as the representative drying temperature. The purpose of followed 200 °C (sample W-50 + 200) was to remove the residual ammonia in order to compare the catalysis of NH_3 during washing with ethanol (i.e., the sample W-50 + 200 ~ E-50 and sample W-50 + 200 ~ E(A)-50). The ammonia was added in washing with ethanol for sample W-50 + 200 ~ E(A)-50, and the amount of ammonia was calculated using 1.5% of N content in sample according to our previous study [24], that was the highest N content in a series of samples after 50 °C drying. Besides, the sample without washing (sample N-50) and the sample washed with ethanol but without drying (sample E-N; measured only by TG/DSC-FTIR because it was wet) were compared at the same time.

Characterization by TG/DSC-FTIR

A simultaneous thermal analyzer (STA 449F3, Netzsch, Germany) including thermogravimetry (TG) and differential scanning calorimetry (DSC) was used to determine thermal properties of all post-treated samples. Each sample (15–25 mg) was heated from 50 to 1200 °C (10 °C min^{-1} heating rate) in a dry air or argon atmosphere. The evolved gas analysis (EGA) was performed through coupling STA with Fourier transform infrared spectroscopy (Vertex 70, Bruker, Germany). The infrared spectra of evolved gases were collected in the mid-infrared range (4000–400 cm^{-1}) with a resolution of 4 cm^{-1}. Also the FTIR transmission spectra of solid samples were determined under similar condition. The spectrum of the representative sample (sample W-50) is presented in Supplementary Material (see Fig. S2), with absorption peaks consistent with the typical spectrum of silica [29, 30].

Elemental analysis and N_2 adsorption

The carbon and nitrogen contents of all samples were measured by an elemental analysis instrument (vario MACRO cube, Elementar Analysensysteme GmbH, Germany). During measurement, the sample was combusted in oxygen at up to 1200 °C. The generated gaseous components are separated by adsorption–desorption columns and subsequently examined by TCD (thermal conductivity

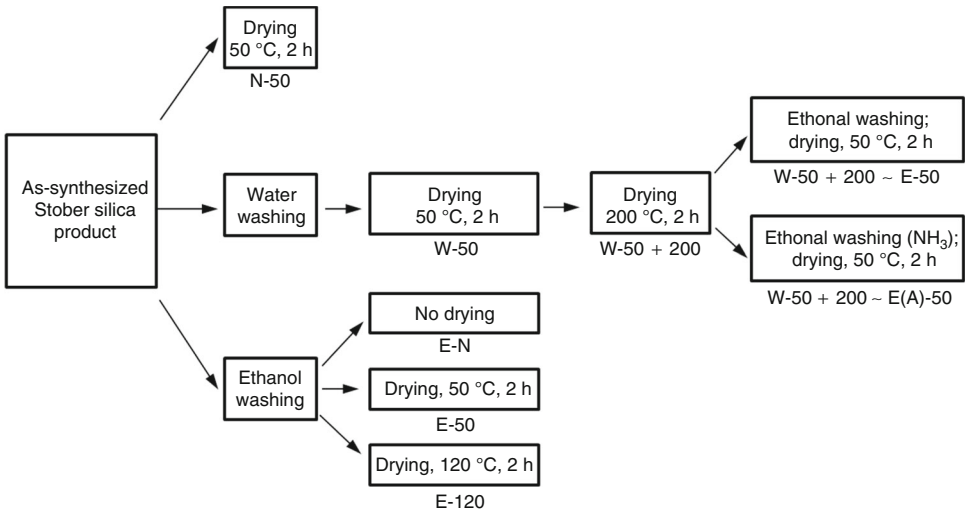

Fig. 1 Flowchart for Stöber silica samples prepared with different post-treatment processes

detector). The result for each sample (20–40 mg) was the average value of two measurements.

Nitrogen adsorption (− 196 °C) was performed using an Autosorb-iQ_2-MP gas adsorption analyzer (Quantachrome, USA). Before measurement, the samples were outgassed at 200 °C for 12 h under vacuum. The N_2 is of 99.999% purity, and the p/p_0 ranged from 10^{-6} to 0.99. Brunauer–Emmett–Teller (BET) and non-local density functional theory (NLDFT) models were used to analyze the specific surface area, pore size, etc. The representative adsorption/desorption isotherms and pore size distributions from NLDFT were displayed in Supplementary Material (see Fig. S3).

Results and discussion

STA characterization of samples with different washing processes

The mass losses from TG, the C, N contents from elemental analysis, and the BET specific surfaces and pore width from NLDFT according to N_2 adsorption for all samples are summarized in Table 1. The STA (TG/DSC) curves of samples washed with water, ethanol and without washing (samples W-50, E-50 and N-50) are presented in Fig. 2, which clearly reveals the obvious effect of solvent washing on Stöber silica's thermal properties.

The mass losses from 50 to 200 °C were resulted from the removal of free or physically adsorbed water, ethanol and ammonia, which was confirmed with the evolved gas analysis and will be discussed in "Effect of drying condition" section. Above 200 °C, the mass loss was due to the removal of surface hydroxyl and ethoxyl groups. The mass loss above 200 °C of sample N-50 (4.8%) is lower than that of sample E-50 (6.2%), which should be caused by the

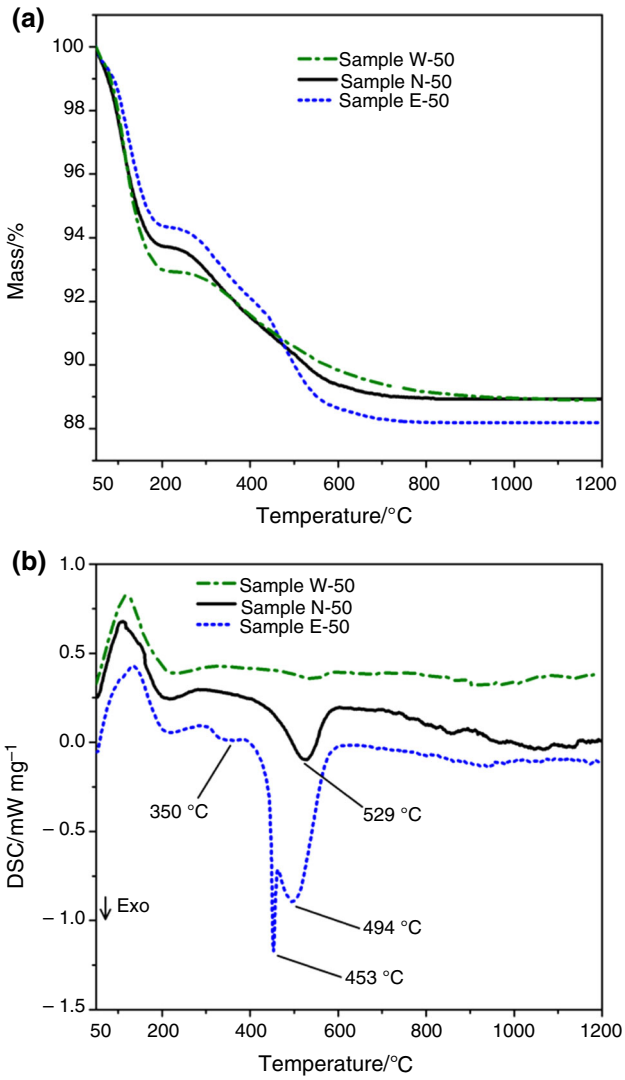

Fig. 2 TG and DSC curves of samples W-50, N-50 and E-50 under air. **a** TG, and **b** DSC

difference in C content. During Stöber synthesis, TEOS could not be completely hydrolyzed, and thus, the residual ethoxyl groups still remained on the particle surface resulting in 0.41% of C in sample N-50 (see Table 1). Since part of the surface hydroxyl (silanol) groups could be esterified to form ethoxyl group during ethanol washing [31–33], the C content of sample E-50 (correspondingly the mass loss above 200 °C) was much higher than that of sample N-50 (see Table 1). Although some investigation pointed out that the esterification of the silanol groups might occur under heating [33], the existence of NH_3 may catalyze the process at lower temperature, which will be further confirmed in "Verification of the catalytic effect of ammonia" section. When washed with water, most of the ethoxyl groups were hydrolyzed and removed from the silica particles, which results in a low C content of 0.04% (see sample W-50 in Table 1). Therefore, the mass loss above 200 °C (4.1%) of sample W-50 is lower than that of the other two samples.

The above-discussed effect of solvent washing is also consistent with the DSC curves (Fig. 2b), with the endothermic peaks from 50 to 200 °C reflecting the removal of volatiles as mentioned earlier and the exothermic peaks above 200 °C representing the oxidation of ethoxyl groups in air. (The endothermic process of removal of surface hydroxyl is weak in such a wide temperature range.) It is straightforward to understand the lack of strong exothermic peak for sample W-50 due to its little ethoxyl groups (0.04% C content). Accordingly, it is reasonable that the exothermic process of sample E-50 (higher C%) is much stronger than that of sample N-50. Besides, there exist two more peaks (a weak one at 350 °C and a sharp one at 453 °C) in sample E-50 than in sample N-50. Based on our previous study [19, 24], water washing is effective in hydrolyzing and removing the pore-blocking materials (including ethoxyl groups and TEOS monomers or oligomers) and leads to cleared micropores combined with suitable drying condition, which enable nitrogen molecules moving in and out smoothly. Therefore, samples with large BET SSA results can be obtained through such a post-treatment process (such as samples W-50, and W-50 + 200 in Table 1). In contrast, because ethanol is unable to hydrolyze the pore-blocking matters and can even exacerbate the pore blocking through ethoxylation (as indicated in Fig. 2), samples washed with ethanol always present small SSA results (such as samples E-50 and E-120 in Table 1). According to Table 1, if pore blocking was effectively cleared (such as samples W-50 and W-50 + 200), the BET SSA could reach 320 $m^2\ g^{-1}$ and was much higher than the geometric SSA ($\sim$ 18.5 $m^2\ g^{-1}$). Thus, it is reasonable to attribute the much weaker exothermic peak at 350 °C for sample E-50 to the oxidization of ethoxyl groups on the outer surface. On the other hand, the absence of obvious oxidation peak at $\sim$ 350 °C for samples N-50 and W-50 is also in line with their much smaller amount of ethoxyl groups (compare C% in Table 1). Accordingly, the much larger exothermic peaks at higher temperature (> 450 °C) should correspond to the oxidation of internal ethoxyl groups on the pore surface [34].

Additionally, we speculate that the sharp peak at 453 °C in the DSC curve of E-50 (instead of N-50 or W-50; see Fig. 2b) should result from sudden (or explosive) release of gases (due to thermolysis of organic matters) from the "sealed" micropores, which accordingly reinforces the aggravated pore-blocking by ethanol washing.

Effect of drying condition

The profound effect of drying condition on Stöber silica's microporosity had been demonstrated through our previous experimentations [19, 24]. In this work, we utilized STA-FTIR technique to improve the mechanistic understanding of the drying effect. We choose to compare the TG, DSC (Fig. 3) and evolved gas analysis (Fig. 4) results for samples E-50, E-120 and E-N, because these ethanol-washed samples display pronounced thermal analysis signals (due to ethoxylation discussed in previous section) which vary with different drying conditions.

The mass loss (Fig. 3a) from 50 to 200 °C was mostly due to residual volatiles (ethanol, ammonia and water) as indicated in Fig. 4. For example, Fig. 4a shows the existence of ethanol and NH_3. (The absorption peak of water is not obvious in Fig. 4a because of the strong absorption peak of ethanol and NH_3.) Figure 4b displays the absorption peaks of water and NH_3, and the absorption peak of water is obvious in Fig. 4c. Accordingly, Fig. 3b exhibits two overlapping endothermic DSC peaks at about 79 and 113 °C (sample E-N; not marked). It is critical to point out the fairly large mass loss (23.9%) from 50 to 200 °C for sample E-N, which signifies substantial material basis for drying-induced reactions (condensation and ethoxylation) for actually all samples (including E-50 and E-120 before drying). After drying at 50 °C (sample E-50), almost all ethanol evaporated and a certain amount of ammonia remained (see Fig. 4b), resulting in a drastically decreased mass loss (5.7%) between 50 and 200 °C (see Table 1) and an endothermic DSC peak at about 117 °C (Fig. 3b; not marked). The hydrogen bond between surface hydroxyl group and ammonia may be the reason of the higher evaporation temperature of ammonia [33]. For sample E-120, no obvious absorption peaks of NH_3 can be found from Fig. 4c, which suggests that the ammonia was removed totally and is consistent with the low N content (0.04%) in Table 1. Thus the mass loss (4.0%) from 50 to

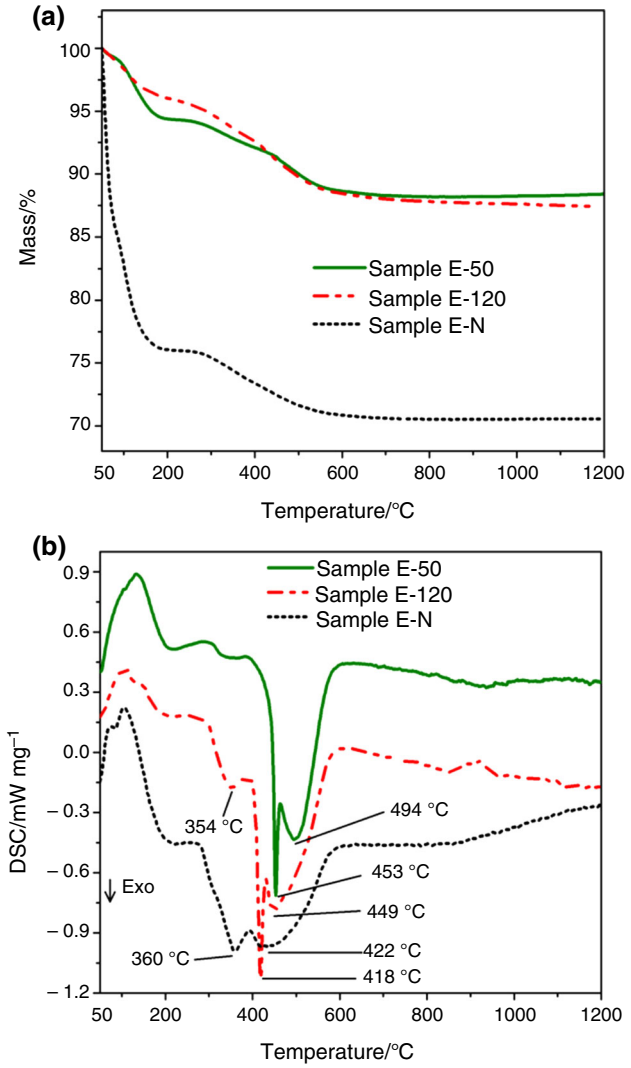

Fig. 3 STA curves of samples E-50, E-120 and E-N under air. **a** TG, and **b** DSC

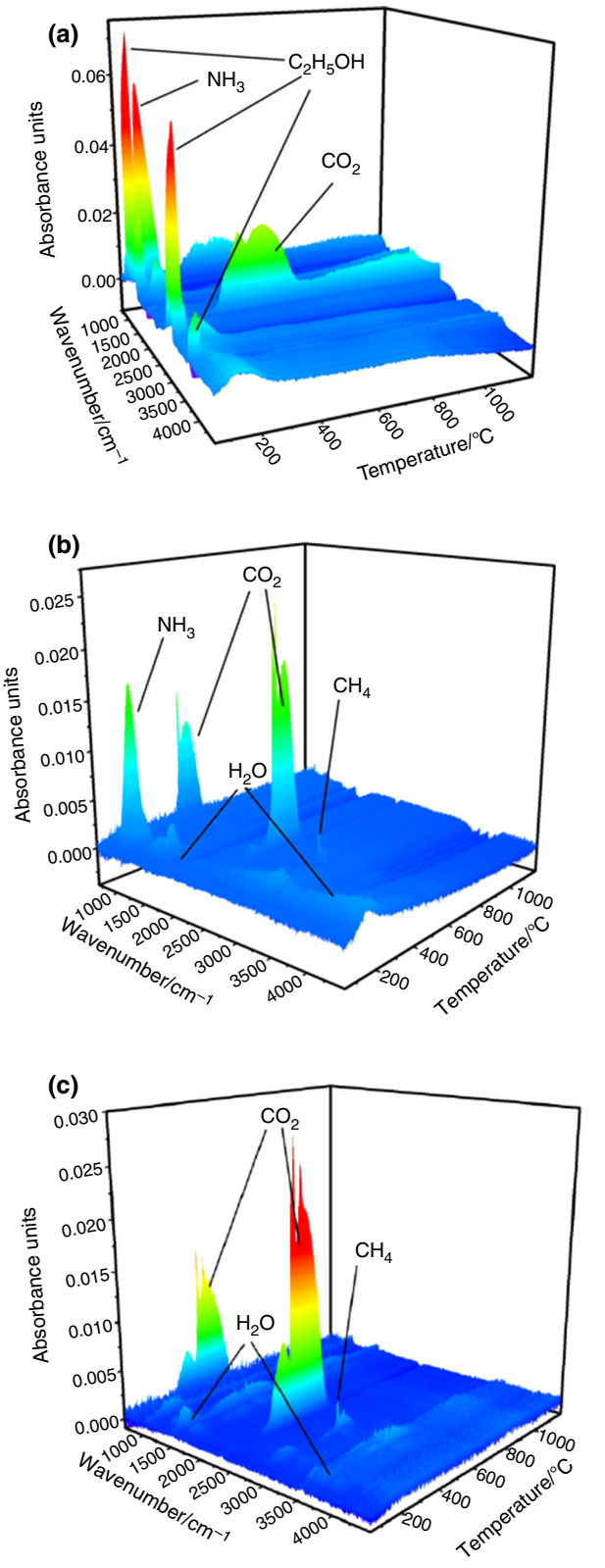

Fig. 4 3D FTIR spectra of evolved gases under air for samples E-N (**a**), E-50 (**b**) and E-120 (**c**) (The filled colors in the figure just display the position of peak more clearly and not indicate other means, and latter figures in the same)

200 °C for sample E-120 was mainly caused by the physically adsorbed water.

The mass loss above 200 °C was due to removal of ethoxyl and hydroxyl groups. As mentioned earlier, the endothermic effect of removal of hydroxyl groups is weak in the wide temperature range (from 200 to 1200 °C); thus, the DSC curve of sample E-N presents two overlapping exothermic peaks (at 360 °C and 422 °C in Fig. 3b) due to the oxidation of ethoxyl groups. For samples E-50 and E-120, the oxidation of ethoxyl groups is also reflected on the DSC curves (Fig. 3b), i.e., 453 °C and 494 °C for sample E-50 and 418 °C and 449 °C for sample E-120, respectively. All the exothermic peaks were resulted from the burning of ethoxyl groups and thus carbon dioxide was identified through the absorption peaks in Fig. 4.

As discussed earlier, our samples (especially before drying) always contain certain residual volatiles, which

may provide the material basis for silanol or ethoxyl condensation reactions catalyzed by NH_3 (more discussion in next section) [32]. The condensation of ethoxyl groups or Si-containing species at pore channels may result in pore blocking to a certain extent depending on the drying condition [19, 24]. Nevertheless, several counteracting factors lead to considerable complexity in understanding the consequence of drying. For example, while higher drying temperature (or longer duration) is normally considered to favor condensation, it also facilitates evaporation of ethanol and ammonia. In Fig. 3b, very similar DSC profiles are found for samples E-50 and E-120. However, the exothermic process (802.5 J g^{-1} from 250 to 620 °C) for E-120 appears stronger than that of E-50 (608 J g^{-1}), consistent with its higher C content (2.42%) than that (1.68%) of E-50, and the DSC peaks for E-120 obviously shift to considerably lower temperatures compared with E-50. Although drying at 120 °C for 2 h almost completely removed NH_3 in E-120 (0.04% of N content in Table 1), it should be recognized that at the start of drying, large amounts of volatiles including ammonia and ethanol comparable to those of E-N (23.9% mass loss from 50 to 200 °C) were available for the NH_3-catalyzed ethoxylation reaction. Because the above reaction proceeds much faster at 120 °C than at 50 °C, the overall extent of ethoxylation (or C content) and thus the DSC peak area for E-120 are larger than those for E-50. There may be two reasons to account for the difference in DSC peak positions. One is that lower drying temperature (i.e., slower reaction rate) should favor ethoxylation forming at silanol sites with higher reactivity, which needs to be removed at higher temperature during STA measurement. The other reason may be that more ethoxylation in sample E-120 should result in an easier buildup and pop out of thermally generated gases at lower temperature from the blocked micropores. For sample E-N, a lot of volatiles (23.9%) and heating during STA measurement should promote ethoxylation. However, because of the relatively quick heating rate (10 °C min^{-1}) and thus short reaction duration before all volatiles evaporate, the extent of ethoxylation and the corresponding exothermic peak area (651 J g^{-1}) lie between those of samples E-50 and E-120. The lack of the sharp DSC peak in sample E-N implies that the pore blocking effect under STA heating condition was not as serious as that in samples E-50 and E-120.

Verification of the catalytic effect of ammonia

In order to further verify that the known catalytic effect of NH_3 on condensation reactions also applies to Stöber silica samples [32], we compared the extent of ethoxylation for samples washed with ethanol but with or without addition of NH_3. Sample W-50 + 200 (water washing followed by drying at 50 and 200 °C; see Fig. 1) was deliberately chosen to test the effect of NH_3, because it contained insignificant ethoxyl and NH_3 contents (C: 0.04%, N: 0.03%; Table 1) but cleared micropores as shown in Table 1 (the BET SSA is 324.3 m^2 g^{-1}). Samples W-50 + 200 ~ E-50 and W-50 + 200 ~ E(A)-50 were obtained through ethanol-washed sample W-50 + 200 with or without NH_3, respectively. The DSC curves for the above three samples are presented in Fig. 5. No obvious exothermic peak can be found in the DSC curve of sample W-50 + 200, consistent with its low C content. For sample W-50 + 200 ~ E-50 (ethanol washed without NH_3), a weak exothermic peak at 486 °C indicates a discernable extent of ethoxylation. The quite large carbon content (1.77%) in sample W-50 + 200 ~ E-50 appears incompatible with the small DSC peak area, indicating that much of the carbon may exist in the form of ethanol molecules in the cleared micropores of this sample (as confirmed in "Evidence of micropore existence in Stöber silica" section). The BET SSA of sample W-50 + 200 ~ E-50 (322.6 m^2 g^{-1}) is close to that of sample W-50 + 200, which also confirm the weak ethoxylation without NH_3 and is consistent with our previous study [19]. In our previous work [19], we discussed that the main pore blocking was caused by the Si-containing monomer or oligomers that could be dissolved in water during washing, and the blocking of ethoxyl groups was minor reason. That is, the BET SSA of sample washed with ethanol is small no matter what drying temperatures because of the small solubility of Si-containing monomer or oligomers in ethanol. After washed with water, the pores channel was cleared (such as samples W-50 and W-50 + 200), the blocking of ethoxyl during ethanol washing (sample W-50 + 200 ~ E-50) is weak especially without NH_3.

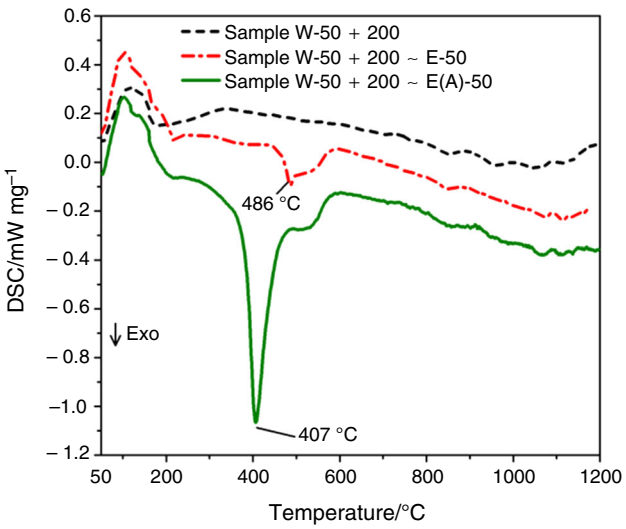

Fig. 5 DSC curves of samples W-50 + 200, W-50 + 200 ~ E-50 and W-50 + 200 ~ E(A)-50 under air

But the longer N_2 adsorption measurement time (88 h) for sample W-50 + 200 ~ E-50 than that (72 h) of sample W-50 + 200 may indicate slight pore blocking in W-50 + 200 ~ E-50. Meanwhile, from the pore size distributions in Figs. S3f, h, the pore width of 0.8 nm in sample W-50 + 200 increase to about 1.3 nm in sample W-50 + 200 ~ E-50, which also imply the slight pores blocking.

In contrast, for sample W-50 + 200 ~ E(A)-50 (ethanol washed with NH_3), there shows a strong peak located at 407 °C besides the peak at ~ 486 °C, which suggests that the NH_3 indeed catalyzes the ethoxylation reaction. The lower temperature (407 °C) of the DSC peak for sample W-50 + 200 ~ E(A)-50 may be due to similar reason accounting for the lowered DSC peak position (418 °C) for sample E-120, as NH_3 catalysis could lower the energy barrier for the reactions between ethanol and less reactive silanol sites. Again, the lack of a sharp DSC peak as in samples E-50 and E-120 suggests that the pore blocking is not very serious in sample W-50 + 200 ~ E(A)-50, which is supported by the N_2 adsorption results described as follows. Although the measurement for sample W-50 + 200 ~ E(A)-50 was not finished because of the long measurement time, the adsorption volume reached 18 $cm^3\ g^{-1}$ at 5×10^{-6} of p/p_0 relative pressure, which was much higher than that of samples E-50 and E-120. That could be explained with the above same mechanism, but for sample W-50 + 200 ~ E(A)-50, the pores blocking was more serious than sample W-50 + 200 ~ E-50 because of the existence of NH_3, so the measurement time was long. Hence, during post-treatment processes or application of Stöber silica, the existence of NH_3 should not be neglected, which influence the pore blocking by catalyzing the ethoxylation reaction.

Evidence of micropore existence in Stöber silica

We also found an interesting phenomenon from the 3D FTIR spectra of the evolved gas analysis, which could further demonstrate the existence of micropores in Stöber silica samples. For sample W-50 + 200 ~ E-50, ethanol was found to evolve out from the temperature range of 130–220 °C (peak ~ 170 °C, see Fig. 6), much higher than the boiling point (78 °C at 1 atmosphere) of ethanol. The same result was also found for sample W-50 + 200 ~ E(A)-50. The elevated gas evolving temperature is consistent with the Kelvin equation [35], which states that the evaporating temperature of liquids confined in nanopores is inversely proportional to the pore size. It may be non-trivial to derive the pore characteristics (shape, size, volume, etc.) about our samples from the EGA results, because the microporous structure formed through aggregation of nuclei can be very complex probably containing

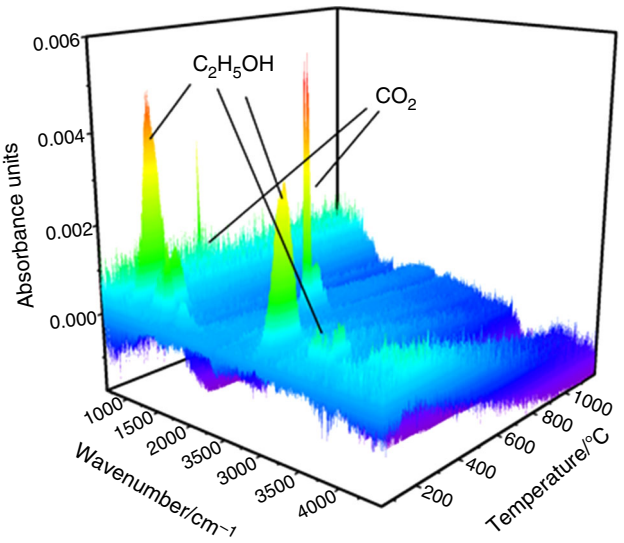

Fig. 6 3D FTIR spectra of evolved gases for sample W-50 + 200 ~ E-50 under air

narrow, tortuous inner pores and clogging surface or inner barriers. Nevertheless, we still believe that the much higher evolving temperature of ethanol is a strong indication of micropores in our samples.

Pyrolysis of organic matters in micropores

The above thermal analysis results were acquired in air atmosphere, and so far we have mainly discussed the oxidization process at high temperature, in which organic matters (ethoxyl groups or ethanol) are converted into CO_2. In fact, CO_2 is not the only gaseous species converted from organic matters in micropores of our samples. For example, a close look at the 3D FTIR spectra of samples E-50 and E-120 reveals that a small amount of methane (CH_4) actually accompanies CO_2 in the evolved gases (see Fig. 4b, c). Although the mechanism can be complicated, the formation of methane, which survives oxidation in air, implies possible catalytic effect of silica micropores on the thermal decomposition of organic matters. We also performed STA-FTIR in argon atmosphere to explore the thermal properties of our samples under anoxic condition. Similar to STA-FTIR measurement in air, heating sample E-50 in argon at ~ 150 °C removed NH_3 as identified in the evolved gases FTIR spectra (Fig. 7a).Yet, some CO_2 still came out in the range of 300–450 °C (Fig. 7a), which indicates that even under argon atmosphere, residual air in the instrument or adsorbed on the sample is still available to oxidize part of the ethoxyl groups. A notable finding for sample E-50 heated under argon atmosphere is the identification of substantial amount of ethylene (C_2H_4) in the 3D FTIR spectra (534 °C in Fig. 7a), which should result from the pyrolysis of ethoxyl groups and is consistent with the

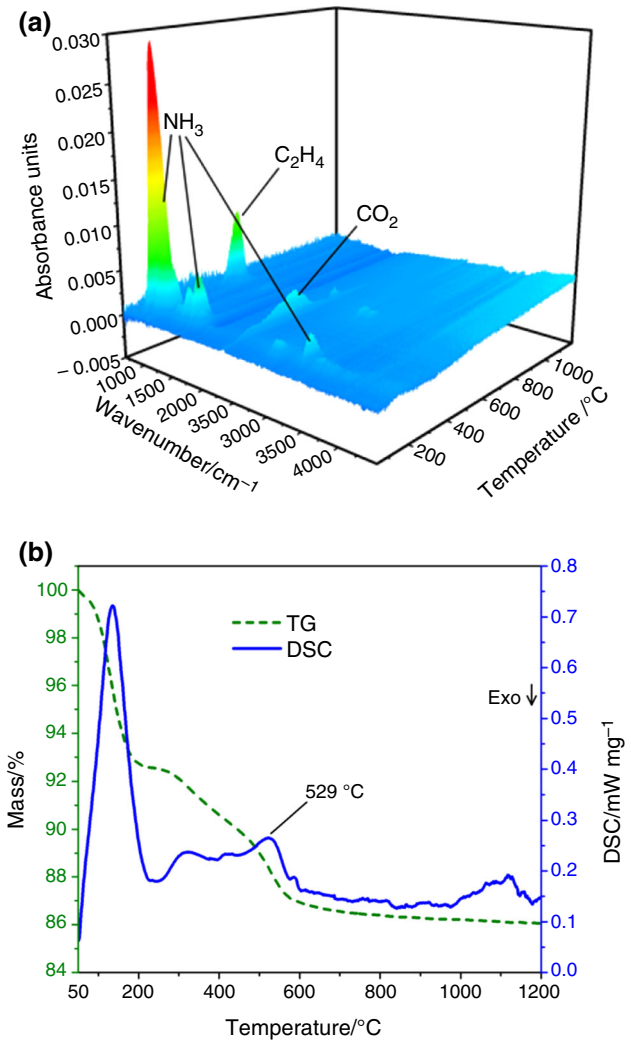

Fig. 7 **a** 3D FTIR spectra, and **b** TG/DSC curves of sample E-50 under argon

endothermic peak in the DSC curve (529 °C in Fig. 7b). These EGA findings demonstrate the intriguing but complex microporous environment of our samples, which may deserve further systematic investigations.

Conclusions

STA-FTIR measurements in this work have demonstrated that washing and drying processes remarkably influence the thermal behaviors (including mass loss, caloric effect, evolved gas, etc.) of Stöber silica samples. Water washing can clear the pores entrance through hydrolysis of ethoxyl groups and Si species (mainly hydrolyzed monomers or oligomers). In contrast, ethanol washing can lead to ethoxylation of silanol groups. Drying may promote the condensation of silanol or ethoxyl and ethoxylation of silanol groups catalyzed by NH_3. Our experimental results indicate that substantial material basis and suitable reaction condition may be available to facilitate the drying-induced ethoxylation between ethanol and silanol groups. More importantly, analysis of our results has provided new insights and strong evidence for the improved understanding of the effects of post-treatments on Stöber silica's microporosity, which are compatible with all SSA and elemental analysis results and thus reinforce the micropore blocking and clearing mechanism in our previous work. The ability of water (or inability of ethanol) to hydrolyze and remove the pore-blocking materials including ethoxyl groups and Si-containing oligomers is emphasized, while the role of ammonia-catalyzed condensation reactions is discussed. Some interesting findings including the very sharp exothermic DSC peaks, high evolving temperature of ethanol and pyrolysis of organic matters are interpreted as special properties related to Stöber silica's micropores. Our work also illustrates the usefulness of thermal analysis techniques in studying nanoporous materials, and undoubtedly an improved understanding of the corresponding porous structures and properties will be of vast benefit to the practical optimization and application of such materials.

Acknowledgements The authors gratefully acknowledge support of this work by the National Natural Science Foundation of China (41473064), the Chinese Academy of Sciences ("Hundred Talents Program"), the State Key Laboratory of Ore Deposit Geochemistry (SKLODG-ZY125-09) and the Doctoral Starting up Foundation of Guizhou Normal University, China.

References

1. Stöber W, Fink A, Bohn E. Controlled growth of monodisperse silica spheres in the micron size range. J Colloids Interface Sci. 1968;26(1):62–9.
2. Wong YJ, Zhu L, Teo WS, Tan YW, Yang Y, Wang C, et al. Revisiting the Stöber method: inhomogeneity in silica shells. J Am Chem Soc. 2011;133(30):11422–5.
3. Wang H, Yu M, Lin CK, Lin J. Core–shell structured SiO_2@-YVO_4: Dy^{3+}/Sm^{3+} phosphor particles: sol–gel preparation and characterization. J Colloids Interface Sci. 2006;300(1):176–82.
4. Cho S-H, Park SY, Kim C, Choi P-P, Park J-K. Stabilization of monodispersed spherical silica particles and their alignment with reduced crack density. Colloids Surf A Physicochem Eng Asp. 2014;441:354–9.
5. Diedrich T, Dybowska A, Schott J, Valsarni-Jones E, Oelkers EH. The dissolution rates of SiO_2 nanoparticles as a function of particle size. Environ Sci Technol. 2012;46(9):4909–15.
6. Kim JM, Chang SM, Kong SM, Kim KS, Kim J, Kim WS. Control of hydroxyl group content in silica particle synthesized by the sol-precipitation process. Ceram Int. 2009;35(3):1015–9.
7. Mueller R, Kammler HK, Wegner K, Pratsinis SE. OH surface density of SiO_2 and TiO_2 by thermogravimetric analysis. Langmuir. 2003;19(1):160–5.
8. Bogush GH, Tracy MA, Zukoski CF. Preparation of monodisperse silica particles control of size and mass fraction. J Non-Cryst Solids. 1988;104:95–106.

9. Giesche H. Synthesis of monodispersed silica powders I. Particle properties and reaction kinetics. J Eur Ceram Soc. 1994;14:189–204.
10. Wang H-C, Wu C-Y, Chung C-C, Lai M-H, Chung T-W. Analysis of parameters and interaction between parameters in preparation of uniform silicon dioxide nanoparticles using response surface methodology. Ind Eng Chem Res. 2006;45(24):8043–8.
11. Hartlen KD, Athanasopoulos APT, Kitaev V. Facile preparation of highly monodisperse small silica spheres (15 to > 200 nm) suitable for colloidal templating and formation of ordered arrays. Langmuir. 2008;24(5):1714–20.
12. Yang M, Wu H, Wu H, Huang C, Weng W, Chen M, et al. Preparation and characterization of a highly dispersed and stable Ni catalyst with a microporous nanosilica support. RSC Adv. 2016;6(84):81237–44.
13. Yu MH, Niu YT, Zhang J, Zhang HW, Yang YN, Taran E, et al. Size-dependent gene delivery of amine-modified silica nanoparticles. Nano Res. 2016;9(2):291–305.
14. Szekeres M, Toth J, Dekany I. Specific surface area of Stöber silica determined by various experimental methods. Langmuir. 2002;18(7):2678–85.
15. Dekany I, Nemeth J, Szekeres M, Schoonheydt R. Surfacial, liquid sorption and monolayer-forming properties of hydrophilic and hydrophobic Stöber silica particles. Colloids Polym Sci. 2003;282(1):1–6.
16. Howard A, Khdary N. Spray synthesis of monodisperse sub-micron spherical silica particles. Mater Lett. 2007;61(8–9):1951–4.
17. Davis PJ, Deshpande R, Smith DM, Brinker CJ, Assink RA. Pore structure evolution in silica gel during aging/drying. IV. Varying pore fluid pH. J Non-Cryst Solids. 1994;167(3):295–306.
18. Filipovic R, Obrenovic Z, Stijepovic I, Nikolic LM, Srdic VV. Synthesis of mesoporous silica particles with controlled pore structure. Ceram Int. 2009;35(8):3347–53.
19. Li S, Wan Q, Qin Z, Fu Y, Gu Y. Unraveling the mystery of Stöber silica's microporosity. Langmuir. 2016;32(36):9180–7.
20. Labrosse A, Burneau A. Characterization of porosity of ammonia catalysed alkoxysilane silica. J Non-Cryst Solids. 1997;221(2–3):107–24.
21. Wan Q, Ramsey C, Baran G. Thermal pretreatment of silica composite filler materials. J Therm Anal Calorim. 2010;99(1):237–43.
22. Wells JD, Koopal LK, de Keizer A. Monodisperse, nonporous, spherical silica particles. Colloids Surf A. 2000;166:171–6.
23. Wang YF. Nanogeochemistry: nanostructures, emergent properties and their control on geochemical reactions and mass transfers. Chem Geol. 2014;378:1–23.
24. Li S, Wan Q, Qin Z, Fu Y, Gu Y. Understanding Stöber silica's pore characteristics measured by gas adsorption. Langmuir. 2015;31(2):824–32.
25. Vanblaaderen A, Vangeest J, Vrij A. Monodisperse colloidal silica spheres from tetraalkoxysilanes: particle formation and growth mechanism. J Colloids Interface Sci. 1992;154(2):481–501.
26. Huang Y, Pemberton JE. Synthesis of uniform, spherical sub-100 nm silica particles using a conceptual modification of the classic LaMer model. Colloids Surf A. 2010;360(1–3):175–83.
27. Stefaniak W, Goworek J, Bilinski B. Pore size analysis by nitrogen adsorption and thermal desorption. Colloids Surf A Physicochem Eng Asp. 2003;214(1–3):231–7.
28. Ma Y, Wang J, Zhang Y. TG-FTIR study on pyrolysis of waste printing paper. J Therm Anal Calorim. 2017;129(2):1225–32.
29. Macan J, Paljar K, Burmas B, Spehar G, Leskovac M, Gajovic A. Epoxy-matrix composites filled with surface-modified SiO2 nanoparticles. J Therm Anal Calorim. 2017;127(1):399–408.
30. Catauro M, Naviglio D, Risoluti R, Ciprioti SV. Sol-gel synthesis and thermal behavior of bioactive ferrous citrate-silica hybrid materials. J Therm Anal Calorim. 2018;133(2):1085–92.
31. Ossenkamp GC, Kemmitt T, Johnston JH. Toward functionalized surfaces through surface esterification of silica. Langmuir. 2002;18(15):5749–54.
32. Iler RK. The chemistry of silica: solubility, polymerization, colloid and surface properties. New York: Wiley; 1979.
33. Yariv S, Cross H. Geochemistry of colloid systems for earth scientists. Berlin: Springer; 1979.
34. Ying JY, Benziger JB, Navrotsky A. Structural evolution of alkoxide silica-gels to glass-effect of catalyst pH. J Am Ceram Soc. 1993;76(10):2571–82.
35. Mitropoulos AC. The Kelvin equation. J Colloids Interface Sci. 2008;317(2):643–8.